Active Galaxies

Asaf Pe'er[1]

April 3, 2017

This part of the course is based, by large, on a series of talks given by Prof. Phil Armitage from the University of Colorado, Boulder. See his webpage, http://jilawww.colorado.edu/∼pja/ Some additions are made based on Refs. [1] - [3].

1. Introduction

Most galaxies have supermassive black holes (BHs) at their centers. The masses of these BHs are typically in the range $10^6 - 10^9\ M_\odot$. The existence of these BHs implies that gas that accretes into them releases a large amount of gravitational potential energy. This will result in luminosity of

$$L = \epsilon \dot{M} c^2, \tag{1}$$

where ϵ is the efficiency, and $\dot{M}$ is the accretion rate. Both the efficiency and the accretion rate vary by several orders of magnitude between the different galaxies.

The existence of accretion produces several observational phenomena. These include:

- Very high luminosity from a point source in the nucleus. The small physical size of the emission region allows rapid variability.
- Broad spectral lines due to the Doppler shift of gas orbiting the BH.
- X-ray emission from high temperature plasma close to the BH.
- Mechanical power in the form of outflows and jets from central regions.

In most powerful active galactic nuclei (AGNs), these phenomena dominate over the starlight. Thus, observations reflect both the **accretion rate** and the **viewing angle** to the central engine.

[1]Physics Dep., University College Cork

2. Classes of AGNs

Mainly from historical reasons, AGNs are classified into numerous types, depending (mostly) upon their luminosity in different wavebands - particularly the optical and radio bands.

2.1. Seyfert Galaxies

This was the first class of AGNs that was identified by Carl Seyfert (1943). Seyfert showed that a small number of nearby galaxies have very bright cores, and show emission lines that are unusually broad - up to 8500 km/s.

Seyfert galaxies are reasonably common - about 1% of spiral galaxies.

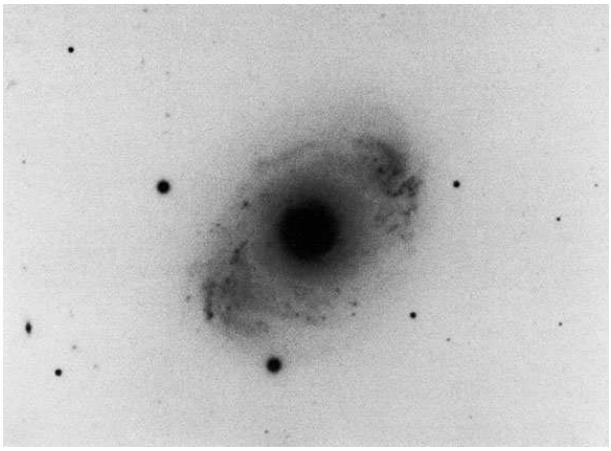

Fig. 1.— The galaxy NGC4151 - one of the original galaxies identified by Seyfert having a bright core.

2.2. Quasars

First radio surveys of the sky were completed in the 1950's. Many prominent radio sources at high galactic latitudes were found to coincide with star-like objects (as appeared on photographic plates). These are named **quasi-stellar radio sources**, or quasars for short.

Their optical spectra did not seem (at first) to match those of known galaxies or other

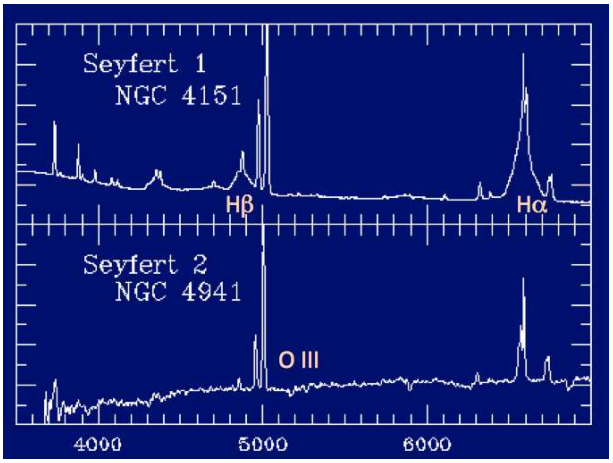

Fig. 2.— Modern spectra of Seyfert galaxies show broad emission lines.

sources. The mystery was solved with the realization that most quasars are in fact distance (luminous) objects, with high redshifted spectra; i.e., their spectra is redshifted by

$$z = \frac{\lambda_{\rm obs}}{\lambda_{\rm emit}} - 1.$$

For example, the brightest known quasar, 3C 273 is at redshift of $z = 0.158$. Using Hubble's law, its distance from us is

$$d = \frac{cZ}{H_0} = 670 \text{ Mpc}.$$

Given its observed brightness (apparent magnitude $m_b = 12.9$ mag), this distance implies an absolute luminosity of ~ 100 times greater than the Milky Way galaxy.

Indeed, shortly after its identifications, Zeldovich & Novikov speculated that massive BH must play a role in producing this luminosity.

Characteristics of quasars include:

- Point-like sources; they were originally detected as radio sources, although the originally detected **radio loud** quasars are actually a small fraction of the total.

- Broad spectral energy distribution (SED), with large UV flux.

  Their spectra cannot be described as a black body, but rather (very crudely) as a power law: $F_\nu = C\nu^{-\alpha}$. Here,F_ν is the specific flux (flux per frequency interval, having units of erg s^{-1} cm^{-2} Hz^{-1}, α is the power law index, C is constant.

The power between frequencies ν_1 and ν_2 is obtained by integrating the flux,

$$P = \int_{\nu_1}^{\nu_2} F_\nu d\nu = \begin{cases} \frac{C}{1-\alpha}\left(\nu_2^{1-\alpha} - \nu_1^{1-\alpha}\right) & \alpha \neq 1 \\ C \ln\left(\frac{\nu_2}{\nu_1}\right) & \alpha = 1. \end{cases} \quad (2)$$

The $\alpha = 1$ spectrum implies equal energy per unit logarithmic frequency interval. Thus, it is most useful to plot AGN spectra using νF_ν as a function of $\log \nu$. (See Figure 3)

- Time variable continuum.
- Broad emission lines (see Figure 2).
- Typically seen at high redshift; as of 2011, the most distant known quasar (ULAS J1120+0641) is at redshift 7.08.

  Note that the high redshift is mainly because quasars are rare and luminous. Even with the best telescopes (HST) it is very difficult to detect the starlight from the host galaxy due to the high luminosity of the nucleus.

3. Evidence for black holes in galactic nuclei

Today, we believe that in the center of most, if not all galaxies there is a supermassive BH, with mass in the range $10^6 - 10^9\ M_\odot$. Clearly, the best evidence for that exist by observations of our own galaxy. Observations clearly indicate individual stars orbiting an unsee companion with a mass of around $3 \times 10^6\ M_\odot$ (see Figure 4). The derived position of the BH coincides with a radio and X-ray source SGR A*, which varies on a short time scale.

A basic question is whether it is possible to prove that the unseen mass is indeed a BH. This is very difficult, as we cannot see directly BH, but we do have indirect evidence. A possible alternative may be a very dense cluster of stars. However, we can use the following argument to rule this out. Given that the observed closest approach of the observed stars to the center is ≈ 130 AU (1 AU $= 1.5 \times 10^{13}$ cm), if we pack $3 \times 10^6\ M_\odot$ in the form of stars inside a sphere of radius $r < 130$ AU, each moving at velocity v, the average time for a given star to collide with other tars is given by

$$t_{\rm coll} \approx \frac{1}{n\sigma_\star v}, \quad (3)$$

where $\sigma_\star = \pi(2R_\star)^2$ is the cross section for a physical collision, and n is the number density of stars. We can estimate these quantities:

$$n = \frac{N_\star}{\frac{4\pi}{3}r^3} = \frac{3 \times 10^6}{\frac{4\pi}{3}(130 \times 1.5 \times 10^{13})^3} \approx 9 \times 10^{-41} \text{ cm}^{-3}, \tag{4}$$

$$\sigma_\star = \pi(2R_\star)^2 \approx 6 \times 10^{22} \text{ cm}^2 \tag{5}$$

where I took $R_\star = R_\odot = 7 \times 10^{10}$ cm. Finally,

$$v \approx \sqrt{\frac{GM_{\rm enclosed}}{r}} \approx 4.5 \times 10^8 \text{ cm s}^{-1} \tag{6}$$

Using these numbers, one finds that $t_{\rm coll} \approx 10$ years !.

This means, that a super-dense cluster of ordinary, solar-type stars would collide almost instantaneously (and, of course, we should be able to see it as well...).

The masses of most black holes cannot be determined to a very high accuracy. Standard methods of determining BH masses include:

1. **Gas disk kinematics.** Measure the velocity of gas disks in the nucleus, correct for inclination, assume Keplerian motion and use $M = rv^2/G$ to estimate mass from observed radius and velocity.

   This works generally well, but the method is less accurate, because: (a) measurements are made much further from the BH (typically, ~ 100 pc). (b) Gas disks may have more complex motions (eccentricity, pressure support, etc.).

2. **Stellar kinematics**. If the velocity dispersion in a galaxy, σ, is known, the BH will dominate motion of stars with a radius $r_{\rm BH}$, which is known as the **Black hole sphere of influence**. It is given by

   $$\sqrt{\frac{GM_{BH}}{r_{BH}}} = \sigma \quad \rightarrow \quad r_{BH} = \frac{GM_{BH}}{\sigma^2} \tag{7}$$

   (the effects on stellar orbits outside this radius are subtle).

   If we can measure the velocities of stars within the sphere of influence (i.e., we have good enough spatially resolved spectra), we expect to see increase in stellar velocities due to the presence of black hole. However, in practice, this is a very difficult measurement; e.g., for $M_{BH} = 10^8\ M_\odot$ and velocity dispersion $\sigma = 200$ km/s, the sphere of influence is $r_{BH} \simeq 11$ pc. Thus, this method is feasible for nearby galaxies, and requires top (HST) resolution (see Figure 5).

This further leads to a tight correlation between the central BH mass and the velocity dispersion, of the form $M = C\sigma^{\alpha}$ with $\alpha \simeq 4$ (compare to the Faber-Jackson relation, $L \sim \sigma^4$).

3.1. A short recap on black holes

Let me briefly overview some basics of black holes (especially for those not taking GR). In the framework of GR, space(-time) is not fixed, but curved. Einstein equation determines how the existence of mass (or energy) acts to curve space-time. A BH represents a solution to Einstein equation, in which part of space time is curved in such a way that in order to get out of this part, one need to travel at speed faster than light, which is impossible.

The **no hair theorem** states that black holes are completely specified by only three quantities: (1) their mass, M; (2) angular momentum, J; and (3) charge, Q. A **Schwarzschild** black hole has $Q = 0$ and $j = 0$, and is therefore spherically symmetric. This solution to Einstein's equation has two important radii:

1. An **event horizon** at $R_g = \frac{2GM}{c^2}$ (known as the **Schwarzschild radius**) represent a point in space out of which no matter, radiation or any information can escape once entered. For a solar mass BH, this radius is $R_g = 3$ km, while for $M = 10^8\ M_\odot$ BH, this radius is $R_g \approx 2$ AU.

2. An **innermost stable circular orbit**, $R_{ISCO} = \frac{6GM}{c^2}$ represents the innermost radius in which circular stable orbits exist. Thus, a test particle at radius $R \geq R_{ISCO}$ from the BH can, in principle, orbit the BH indefinitely. However, at $R < R_{ISCO}$, all the orbits are unstable, and particles will inevitably spiral rapidly past the event horizon and into the BH.

   R_{ISCO} therefore defines the inner edge of the gas disk in AGN. This, in turn, sets a minimum orbital period. Roughly,

$$t = \frac{2\pi R_{ISCO}}{v_{ISCO}} = \frac{2\pi R_{ISCO}}{\sqrt{\frac{c^2}{6}}} = 12\sqrt{6}\pi\frac{GM}{c^3} \tag{8}$$

   (note that this derivation is based on Keplerian motion in Newtonian potential, so it is not exact, but still gives the correct order of magnitude).

   For $M_{BH} = 10^8\ M_\odot$, this time is about 12 hours (for $M = 10\ M_\odot$ this is ~ 5 ms). One therefore does not expect any period signal on a shorter time.

A second type of solution is that with $Q = 0$ while $J \neq 0$. This is known as **Kerr** black hole. This solution is not spherically symmetric, but rather is axisymmetric, namely the BH has a preferred rotation axis. The amount of angular momentum is defined via a dimensionless **spin parameter**,

$$a = \frac{cJ}{GM^2}. \tag{9}$$

The maximum angular momentum of a Kerr BH therefore corresponds to a spin parameter $a = 1$, which is the absolute theoretical limit on the spin of a BH of mass M.

Similar to Schwarzschild BHs, Kerr BHs also have an event horizon and an innermost stable circular orbit. For particles orbiting in the equatorial plane of the H, $R_{ISCO}(Kerr) < R_{ISCO}(Sch.)$ if the orbit co-rotates with the BH, but is larger for counter-rotation. This means that gas in the disk around Kerr BH can spiral deeper into the potential well before reaching R_{ISCO}. As a result, more gravitational energy can be extracted.

3.2. Eddington limit and fueling of black holes in AGNs

For an AGN with observed bolometric luminosity L, one can estimate the *minimum* mass of the BH involved. This is done by assuming that the gas around BH is (1) spherically symmetric and (2) composed of fully ionized hydrogen.

For an object at distance r, the observed energy flux is $F = \frac{L}{4\pi r^2}$. Since the momentum of a photon having energy E is E/c, the **momentum flux** due to radiation is $P_{rad} = \frac{L}{4\pi r^2 c}$. This is equal to the **pressure** that would be exerted on a totally absorbing surface at distance r from the source.

The force exerted on the gas depends upon the opacity (the fraction of the radiation absorbed by the gas). The minimum force is given by the absorption due only to free electrons. For this process, the cross section is Thomson cross section, $\sigma_T = 6.65 \times 10^{-25}$ cm^2. Therefore, the outward radiation force on a single electron is

$$F_{rad} = \frac{L\sigma_T}{4\pi r^2 c}. \tag{10}$$

On the other hand, the inward force is due to gravity, and given a mass M at the center it is

$$F_G = \frac{GM(m_p + m_e)}{r^2} \approx \frac{GMm_p}{r^2} \tag{11}$$

where in the calculation we considered the fact that gravity acts on the protons as well, and that the electrons and protons are coupled by the electrostatic force.

Setting $F_G = F_{rad}$, one thus gets

$$L = \frac{4\pi G c m_p}{\sigma_T} M = 1.26 \times 10^{38} \left(\frac{M}{M_\odot}\right) \text{ erg s}^{-1}. \tag{12}$$

This luminosity is known as **Eddington limit**. It is the maximum luminosity of a steady source of mass M, which is powered by spherical accretion of gas.

One can invert the argument: If a source with observed luminosity L is radiating at the Eddington limit, its mass would be

$$M_{Edd} = 8 \times 10^5 \left(\frac{L}{10^{44} \text{ erg s}^{-1}}\right) M_\odot \tag{13}$$

This is a minimum limit on the mass: the source could actually be radiating at much less than the Eddington limit.

A luminous Seyfert galaxy has $L \sim 10^{44}$ erg s^{-1}. Thus, we conclude that the BH mass in those galaxies must be at least 10^6 $M_\odot$, i.e., could be comparable to the BH in the center of the Milky Way.

For quasars, $L_{QSO} \sim 10^{46}$ erg s^{-1}. The BH mass in those systems must be at least $\sim 10^8$ $M_\odot$.

The next question, is how fast must a gas be supplied to a BH to produce a typical AGN luminosity of $10^{44} - 10^{46}$ erg/s ?. This depends on the efficiency of the accretion process, η, which we can define via

$$L = \eta \dot{M} c^2. \tag{14}$$

Here , $\dot{M}$ is the accretion rate.

A mass δm of gas at infinity has zero potential energy. Thus, the available energy if the gas spirals in to radius r is

$$\delta E = \frac{G M_{BH} \delta m}{r} \quad \rightarrow L \approx \frac{G M_{BH} \dot{M}}{r}. \tag{15}$$

This of course represents only an upper limit, as not all the potential energy will be radiated as the gas falls in.

An order of magnitude estimate of the efficiency can be obtained by assuming that the gas falls into the innermost stable orbit, at $r = 6GM/c^2$ before being swallowed by the BH. Efficiency estimate will be

$$\eta = \frac{G M_{BH} \dot{M}}{6 G M_{BH}/c^2} \times \frac{1}{\dot{M} c^2} \approx 0.17 \tag{16}$$

Although clearly, this Newtonian calculation is very crude, it still gives the correct order of magnitude. Full GR calculation gives efficiency of $\eta = 0.06$ for Schwarzschild BH, and as high as $\eta = 0.42$ for Kerr BH. Thus a standard estimate is $\eta = 0.1$. Using this value, the mass flow needed to sustain a quasar is

$$\dot{M} \approx \frac{10^{46} \text{ erg s}^{-1}}{0.1c^2} \approx 10^{26} \text{ gr s}^{-1} \approx 2 \ M_\odot/yr. \tag{17}$$

Thus, the mass supply is in fact fairly modest.

4. Structure of the accretion disk

The luminosity of AGNs is derived from gravitational potential energy released as gas spirals inward through an **accretion disk**. Here, we briefly derive the basic structure of the disk, and characteristic temperatures of the gas.

Let us consider the vertical structure of the disk. For this, we work in cylindrical coordinates, R, ϕ and z. Let us consider a gas element at radius R and height z above the disk midplane. Denote by $r = \sqrt{R^2 + z^2}$ the distance between the gas element and the central BH, and by θ the angle between r and z.

Assuming $z \ll R$, the gravitational acceleration of the gas element in the vertical direction is

$$g = \frac{GM}{r^2} \cos\theta = \frac{GM}{r^2} \frac{z}{R} \approx \frac{GM}{R^3} z \tag{18}$$

The gas is supported against gravity by a pressure gradient. Force balance in the vertical direction gives

$$\frac{dp}{dz} = -\rho g \tag{19}$$

We can assume that the disk is isothermal in the vertical direction, with speed of sound c_s. Thus, the pressure is given by

$$p = \rho c_s^2 \tag{20}$$

For disk with angular velocity $\Omega = v_\phi/r$, the vertical disk structure will be

$$c_s^2 \frac{d\rho}{dz} = -\rho \frac{GM}{R^3} z = -\Omega^2 \rho z, \tag{21}$$

or

$$\int \frac{d\rho}{\rho} = -\frac{\Omega^2}{c_s^2} \int z dz \tag{22}$$

from which

$$\rho = \rho_0 e^{-\frac{\Omega^2 z^2}{2c_s^2}} = \rho_0 e^{-z^2/h^2}, \tag{23}$$

where $\rho_0 = \rho(z = 0)$, and h is the vertical scale height of the disk,

$$h^2 \equiv \frac{2c_s^2}{\Omega^2} \approx \frac{2c_s^2 R^2}{v_\phi^2} \tag{24}$$

or

$$\frac{h}{R} \approx \frac{c_s}{v_\phi} \tag{25}$$

Thus, the thickness of the disk as a function of radius is given by the ratio of the sound speed to the orbital velocity.

A disk for which $(h/R) \ll 1$ is described as **geometrically thin** disk. Structure of thin disks is relatively simple, because radial pressure forces can be neglected - namely, v_ϕ for the gas is the same as that of a particle orbiting at the same radius.

4.1. Angular momentum transport

If the disk is thin, then the orbital velocity of the gas is Keplerian,

$$v_\phi = \sqrt{\frac{GM}{R}}. \tag{26}$$

The specific angular momentum, $v_\phi R$ is $l = \sqrt{GMR}$. Thus, the specific angular momentum increases outwards. Gas at large radii R has too much angular momentum to be accreted by the BH.

In order to flow inward, gas must lose angular momentum. This can happen either by:

1. By **redistributing** the angular momentum within the disk (gas at small R loses angular momentum to gas further out, and thereby flow inward).

2. By loss of angular momentum from the entire system. For example, wind from the disk could take away angular momentum, allowing inflow.

The redistribution of angular momentum within a thin disk is a *diffusive* process. A narrow ring of gas spreads out under the action of the disk **viscosity**. As time increases, the **mass** all flows inward to small R and is accreted; the **angular momentum** is carried out to very large R by a vanishingly small fraction of mass.

4.2. Radiation from thin accretion disk

Consider a gas flowing inward through a thin disk. Let us now estimate the radial distribution of the temperature. The calculation is as follows.

The potential energy per unit mass at radius R is the disk is

$$E = -\frac{GM}{R} \quad \rightarrow \quad \frac{dE}{dR} = \frac{GM}{R^2} \tag{27}$$

Suppose that a mass dM flows inward a distance dR. The change in potential energy of this mass element is

$$\Delta E = \frac{GM}{R^2} dM dR \tag{28}$$

Half of this energy goes into increased kinetic energy of the gas. If the other half of the energy is radiated, the luminosity will be

$$L = \frac{GM\dot{M}}{2R^2} dR \tag{29}$$

The radiating area is a ring of area $2 \times 2\pi R \times dR$ (the first factor of 2 comes from both sides). The luminosity per unit are is equal to the rate of energy loss via black body radiation,

$$\frac{GM\dot{M}}{8\pi R^3} = \sigma_{SB} T^4 \quad \rightarrow \quad T = \left(\frac{GM\dot{M}}{8\pi\sigma_{SB} R^3} \right)^{1/4} \tag{30}$$

where σ_{SB} is Stefan-Boltzmann constant.

This simple argument gives the correct dependence on the mass, accretion rate ($\dot{M}$) and radius, but the wrong prefactor. More accurate calculation will account for: (a) Radial energy flux through the disk (transport of angular momentum implies transport of energy as well); (b) Boundary conditions at the inner edge of the disk; and (c) GR effects.

After the correction, the radial distribution of the temperature is

$$T(R) = \left(\frac{3GM\dot{M}}{8\pi\sigma_{SB} R^3} \left\{ 1 - \sqrt{\frac{R_{in}}{R}} \right\} \right)^{1/4} \tag{31}$$

where R_{in} is the radius of the disk's inner edge. For $R \gg R_{in}$, Equation 31 simplifies to

$$T(R) = \left(\frac{3GM\dot{M}}{8\pi\sigma_{SB} R_g^3} \right)^{1/4} \left(\frac{R}{R_g} \right)^{-3/4} \tag{32}$$

where $R_g = 2GM/c^2$ is the Schwarzschild radius.

For a BH accreting at the Eddington limit, we saw that the accretion rate scales linearly with mass ($L \propto \dot{M}$ and $L_{\rm Edd} \propto M$); the Schwarzschild radius also scales linearly with mass. Thus, from Equation 32 it follows that the temperature at a fixed number of R_g decreases as $M^{-1/4}$. Thus, **disks around more massive BHs are cooler**.

For supermassive BHs, we can re-write the temperature in Equation 32 as

$$T(R) \approx 6.3 \times 10^5 \left(\frac{\dot{M}}{\dot{M}_E}\right)^{1/4} \left(\frac{M}{10^8 M_\odot}\right)^{-1.4} \left(\frac{R}{R_g}\right)^{-3/4} \text{ K.} \quad (33)$$

where $\dot{M}_E$ is the accretion rate at the Eddington limiting luminosity (assuming $\eta = 0.1$).

Since a thermal spectrum at temperature T peaks at a frequency $h\nu_{\rm max} \approx 2.8 k_B T$, an inner disk temperature of $\sim 10^5$ K corresponds to strong emission at frequencies of $\sim 10^{16}$ Hz, or about 50 nm. Thus, disk emission in AGN accreting at close to the Eddington limit is expected to be strong in the ultraviolet, explaining the origin of the broad peak in quasar SEDs in the blue and UV.

At higher frequencies, an exponential cutoff is expected, while at lower frequencies the spectrum is a weighted sum of many blackbody spectra of different temperatures emitting from different disk regions.

5. Classification and unified model of AGNs

We already encountered two types of AGNs: Seyfert galaxies (which have two types, known as Type I and Type II) and Quasars. Additional types are **BL Lacs** and **Optically Violent Variables (OVVs)**; and radio galaxies, which come in 'broad line' and 'narrow line' variants.

One thing in common to all these types is that they are all powered by accretion onto a supermassive BHs. This raises the question of why there are so many classes - are these physically distinct objects?

To these we should add another class of galaxies, known as **LINERs** (low-ionization nuclear emission-line region galaxies). These are much more common than the other classes, but have very low luminosities.

- **Seyfert galaxies** are lower luminosity AGNs, normally found in spiral galaxies. They are sub-divided into two subclasses: **Type I Seyfert** galaxies have two sets of emission

lines in their spectra: (a) **narrow lines**, with a width (measured in velocity units) of several hundreds km/s; and (b) broad lines, with widths up to 10^4 km/s,

Type II Seyfert galaxies are similar to type I, but show only the narrow line component.

- **BL Lacs** are named after the prototype, BL Lacertae. They are distinguished by lack of a strong emission *or* absorption lines in their spectra.

  A related class of objects are the **optically violent variables (OVVs)**. Many AGNs are variable, but OVVs show larger variations (¿0.1 mag) in optical flux on short timescales (of about a day).

  Collectively, OVVs and BL Lacs are called **blazars**. These can be observed over the entire EM spectrum, from radio to $\gamma-$rays. All known blazars are radio sources.

- **Quasars** are the most luminous subclass of AGNs. A small fraction, $\sim 5-10\%$ are the strong radio sources which originally defined the quasar class. In these objects, nuclear emission normally dominates the host galaxy light.

  Their spectra is very similar to Seyfert galaxies, except that (a) stellar absorption lines are very weak, or cannot be detected; and (b) objects that are called quasars are all 'type I' is the Seyfert jargon - i.e., broad emission lines are always detected.

- **Radio galaxies** are strong radio emitters, that are typically associated with giant elliptical galaxies. Two types of radio galaxies have optical spectra that show AGN activity: (a) broad-line radio galaxies (similar to Type I Seyfert), and (b) narrow line radio galaxies (similar to Type II Seyfert).

  Basically, these objects look like radio loud Seyferts, **but** they seem to occur in ellipticals rather than spiral galaxies.

5.1. Unified model

In order to imposed some order in the mess, there is one additional clue. Crucial observational realization is that emission from the nuclear region is not spherically symmetric. On observational scale (typically $\sim$ pc in nearest AGNs), nuclear often has axial symmetry (see Figure 6).

A unified model seek to explain the different classes of AGNs as being due to different orientations of intrinsically similar systems towards the observer line of sight.

According to this unification scheme, the difference between Seyfert I and Seyfert II galaxies originates from the obscurration of the broad emission line region by an obscuring **torus**. Thus, while the observer of Seyfert I galaxy is not affected by the torus, that of Seyfert II is affected by it (see Figure 7). This unification is considered fairly secured.

According to this picture, we can see the continuum emission in Seyfert II galaxies, despite the fact that it originates from a disk at smaller radii than the broad lines, as above and below the disk plane there is a scattering medium (e.g., electrons) that scatter some of the radiation into our line of sight. A support for this picture originates from the observational fact that in some Seyfert II galaxies, the polarized emission does show broad lines; this is consistent, as scattered emission is polarized.

This picture thus suggests that at least some Seyfert II galaxies are intrinsically similar to Seyfert I. If this applies to all Seyferts, then statistics means that the torus must block about 3/4 of the sky as seen from the nucleus.

It is reasonable to put quasars (Types I and II) as well as blazars into this picture. Quasars will differ from Seyferts by higher accretion rates, but not by viewing angle; Blazars would be viewed directly down the jet.

A more ambitious unification scheme aims at explaining why some AGNs are radio loud, while others are radio quiet. Possible physical difference is the spin of the black hole. Radio loud quasars will be characterized by high spin ($a \sim 1$), which also produce jets - that are the origin of the radio emission. These jets are powered by the spin energy extracted from the black hole.

Contrary, in radio quiet galaxies the spin of the central BH is low, $a \ll 1$, there are no jets and the spectrum is entirely produced by the accretion disk (black body plus non-thermal coronal emission).

6. Measuring the spin of black holes

Measurements of the spin of black holes is important, yet very difficult task. The spin only affects the **local** structure of space-time around the BH. There are several possible routes to measure BH spin, and they are all based on the fact that the inner most stable circular orbit, R_{ISCO} depends on the spin parameter, a: $R_{isco} = 6GM/c^2$ for $a = 0$ (Sch. BH); and is getting smaller (but always $> GM/c^2$) as $a \to 1$.

Existing methods to estimate the BH spin include the following:

- **Luminosity.** For the same accretion rate, rapidly spinning BH will be more luminous than non-rotating one; for Sch. BH, $\eta = 0.06$, while for near maximally spinning Kerr BH, $\eta \sim 0.3$.

- **Variability.** The shortest orbital period for Kerr BH is less than that for a Sch. BH. The rotation also introduce other effects (e.g., frame dragging) that may show up in variability measurements.

- **Velocity.** The highest velocities in the disk are greater for a Kerr BH than a Sch. BH. This is observable if one can measure spectral line produced in the inner disk.

Let us have a closer look at spectral lines from the inner disk. In the Newtonian case, if we consider an annulus in the disk with orbital velocity v_ϕ, the projected velocity is $v_\phi \sin i$, where i is the inclination. This leads to Doppler shift, as $\Delta\nu/\nu = \nu_{ob.}/c$. This leads to a 'double horned' profile.

In relativistic disk, there are additions: (a) the observed frequency is reduced compared to the rest frame value by a factor $\gamma = (1-\beta^2)^{-1/2}$; (b) Beaming boosts blue wing of the line, while attenuating the red ring; and (c) gravitational redshift further shifts the entire profile to lower energies. Finally, integrating over the entire disk radii provides the prediction of **broad, assymetric line profile with sharp cutoff at high** E (see Figure 8).

The inner disk is too hot to produce spectral lines in the optical. In some Seyfert galaxies, detect fluorescent **iron line** in the X-ray spectrum. This line originates from radiating cold (i.e., not fully ionized) disk by hard X-ray photons. This leads to the ejection of an electron from the ground state. An electron from level $n = 2$ drops into the ground state. The excess of energy is emitted as a photon at energy 6.4 keV. While a range of photon energies can eject an electron, the emitted photon is always at a single energy. This leads to **strong emission line**. The iron line is always the strongest line that is observed.

The detection of (broadened) iron lines is, to date, the best 'proof' for the presence of BHs in AGNs.

7. Radio galaxies and relativistic jets

High resolution observations of radio galaxies often show highly extended emission (see Figure 9 of the radio galaxy Cygnus A). The emission is due to synchrotron emission. The physical extend can be very large, and extend up to several hundred kpc.

Observationally, there are two types of radio galaxies.

- **FR-I** (stands for Fanaroff & Riley class I): the separation between the points of peak intensity in the lobes is *less* than half the largest size of the source.
- **FR-II** (Fanaroff & Riley class II): the separation between the points of peak intensity in the lobes is *more* than half the largest size of the source.

Morphological classification also divides the radio galaxies into low radio power and high radio power, with break power at about 10^{32} erg s^{-1} Hz^{-1} sr^{-1}. FR I have relatively low power, while FR II are more powerful sources.

It is believed today that these outflows from AGNs could play an important role in galaxy and / or cluster formation, as it provides an energy source into the ISM or intracluster medium, and the gas flow could be more important than radiation, which can escape the galaxy or cluster more easily.

7.1. Superluminal motion

On small scales, jets near the nucleus often show hotspots, or 'knots' which can be seen to move in time. While it is not certain that the motion of these knots reflects the physical speed of the jet, if it does, the inferred velocity in the plane of the sky exceeds the speed of light. This is known as **superluminal motion**.

The explanation to the apparent superluminal motion is that it is really an optical illusion, caused by the finite speed of light. Consider a knot in the jet moving almost directly towards the observer at high speed. Assume that at time $t = 0$, a blob of gas is emitted, at velocity v making an angle θ to the line of sight. At time δt later, the blob has moved to position which is $v\delta t$ away from its origin. The projection on the line of sight corresponds to distance $v\delta t \cos\theta$, and perpendicular to the line of sight it is $v\delta t \sin\theta$. Thus, the time difference between a photon emitted by the blob at $t = 0$ and at δt is

$$\delta t^{ob} = \delta t(1 - \beta\cos\theta) \tag{34}$$

where $\beta = v/c$. The observer infers a transverse velocity of

$$\beta_T = \frac{vsin\theta}{c(1 - \beta\cos\theta)} = \frac{\beta\sin\theta}{1 - \beta\cos\theta}. \tag{35}$$

For β close to 1 and small θ, one can clearly get an apparent transverse velocity $\beta_T > 1$.

It is straightforward to show that the maximum angle for which β_T is maximal is $\theta_{\max} = \cos^{-1}\beta$, and that $\beta_T^{\max} = \gamma\beta$. Equating this to unity gives the minimum velocity for which superluminal motion is possible, $\beta_{\min} = 1/\sqrt{2} \simeq 0.707$.

The overall conclusion is that the motion of jets do not need to be highly relativistic, in order for superluminal motion to be observed. As a final remark, please note that the apparent superluminal motion is really a geometrical effect, as we did not make any use in any aspect of special relativity in deriving it (except the restriction $v < c$).

REFERENCES

[1] H. Mo, F. van den Bosch and S. White, *Galaxy Formation and Evolution* (Cambridge), chapter 11.

[2] J. Binney and S. Tremaine, *Galactic Dynamics* (Princeton), chapter 6

[3] L.S. Sparke and J.S. Gallagher, *Galaxies in the Universe* (Cambridge), chapter 2

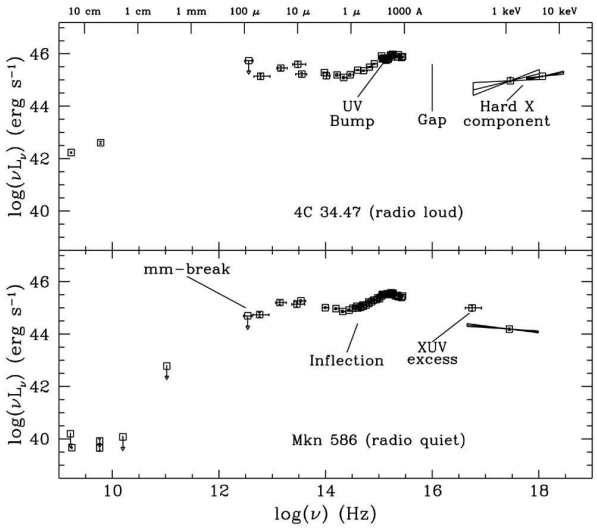

Fig. 3.— Examples of fairly well-observed SEDs for both a radio-quiet (RQQ) and a radio-loud (RLQ) quasar. Both classes show peaks in their energy output in the infra-red (IR bump) and optical ("Big Blue Bump") wavebands. The IR bump is generally attributed to thermal emission from dust at a wide range of temperatures, $\sim 50-1000$ K and the Big Blue Bump in thermal emission from the gas in an accretion disk. The relative strengths of the IR and Big Blue bumps varies but they are generally comparable. The inflection between the two peaks, at $\sim 1.5\mu m$, is due to the maximum dust temperature of ~ 2000K caused by sublimation. In the X-ray region, 50% of both RLQs and RQQs have a soft X-ray excess component thought to be the high energy tail of the Big Blue Bump. The most notable difference between RLQs and RQQs is in the radio waveband. In RQQs the SED turns over sharply in the far-IR/mm and radio emission is $\sim 100-1000\times$ weaker than in RLQs. In RLQs the IR-radio continuum is smooth with non-thermal emission contributing in both wavebands.

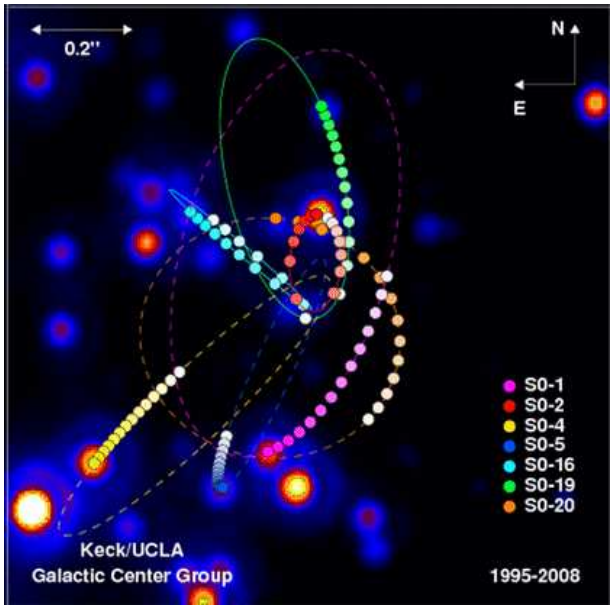

Fig. 4.— Orbits of stars near the Milky Way's galactic center taken over a period of 13 years (1995-2008) show clear ellipses indicating a supermassive BH.

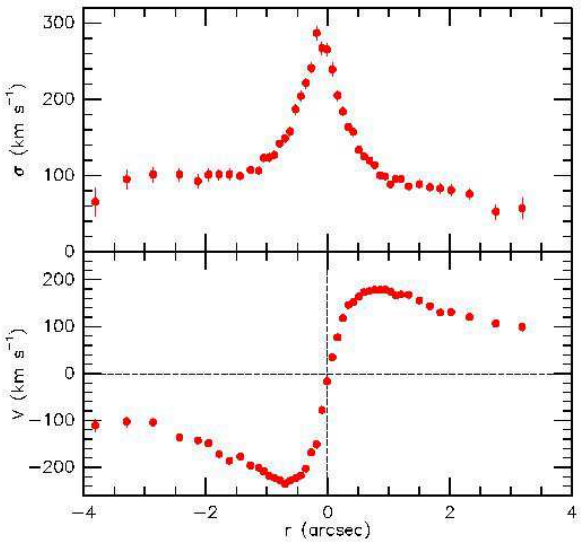

Fig. 5.— Rotation curve (bottom) and velocity dispersion profile (top) of the nucleus with foreground bulge light subtracted of the galaxy M31 (the Andromeda galaxy). There is a clear rise in the velocity dispersion within the central arc-second.

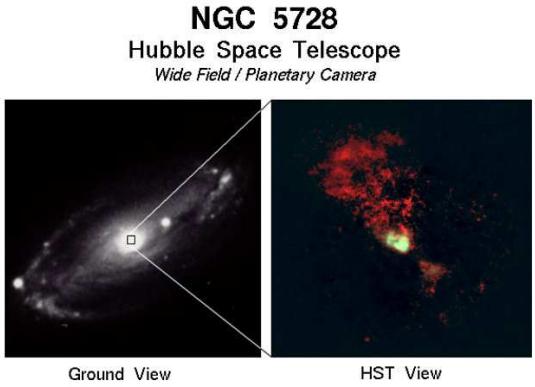

Fig. 6.— HST image of the inner region of NGC5728 shows that the radiation is escaping a conical region, and that something blocks the emission on the perpendicular axis.

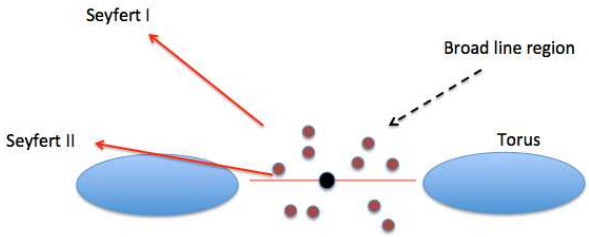

Fig. 7.— Cartoon showing the effect of the viewing angle on the classification of Seyfert galaxies.

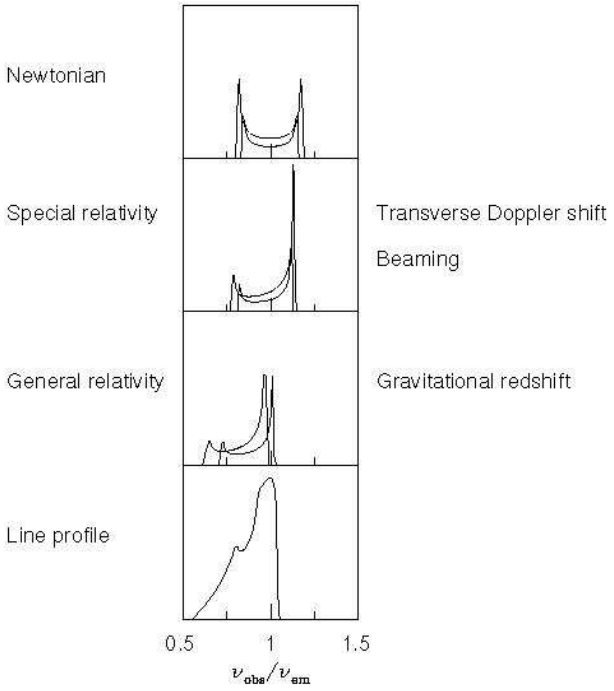

Fig. 8.— The profile of the broad iron line is caused by the interplay of Doppler and transverse-Doppler shifts, relativistic beaming and gravitational redshifting.

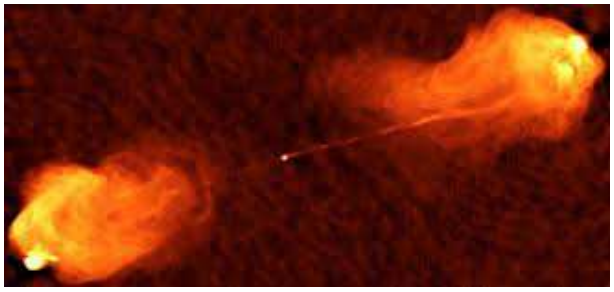

Fig. 9.— The radio galaxy Cygnus A (3C 405), one of the strongest radio sources in the sky as seen at 4.8 GHz (by VLA). Images of the galaxy in the radio portion of the electromagnetic spectrum show two jets protruding in opposite directions from the galaxy's center. These jets extend many times the width of the portion of the host galaxy which emits radiation at visible wavelengths. At the ends of the jets are two lobes with "hot spots" of more intense radiation at their edges. These hot spots are formed when material from the jets collides with the surrounding intergalactic medium. The nucleus, jets, lobes and hotspots are clearly visible.

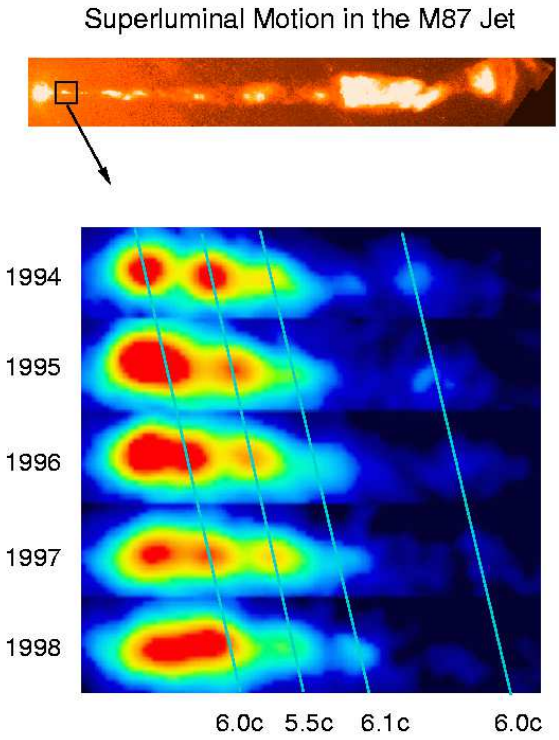

Fig. 10.— Superluminal motion in the M87 jet.